Theoretical Calculations for Elastic and Thermodynamic Properties of NbN_2 under High Pressure

Bao-Sen Hou[a], Ke Liu[a,b,*], Xiao-Chun Mao[a], Jiao Tan[a] and Xiao-Lin Zhou[a]
[a]College of Physics and Electronic Engineering, Sichuan Normal University, Chengdu 610101, P.R. China
[b]School of Micro-Electronics and Solid-State Electronics, University of Electronic Science and Technology, Chengdu 610054, P.R. China

(Received March 31, 2017; in final form July 29, 2017)

The structural and elastic properties of NbN_2 at high pressures were investigated through the first-principles calculation. Results indicate that NbN_2 is a potential hard material. NbN_2 meets mechanical stability criteria and possesses ductility within the pressure of 100 GPa. The elastic anisotropy under high pressure was achieved by the elastic anisotropy factors, which reduce with increasing pressure. Using the quasi-harmonic Debye model, we also investigated the thermodynamic properties of NbN_2.

DOI: 10.12693/APhysPolA.132.1363

PACS/topics: high temperature and high pressure, elastic constants, anisotropy, Debye temperature, NbN_2

1. Introduction

The transition metal nitrides (TMNs) become more and more important in various industrial applications owing to their outstanding and unique physical properties, such as chemical and thermal stabilities, high hardness and strength, high melting point, good thermal and electronic conductivity, and superconductivity [1–3]. Some noble metal nitrides with orthorhombic marcasite-type structure (space group of *Pnnm*, No. 58) such as PtN_2 [4, 5], IrN_2 [5, 6], OsN_2 [6] and PdN_2 [7] with moderate synthesis conditions and very large bulk modulus (close to 400 GPa) are expected to be alternative materials to traditional superhard materials that are of synthesis expensive [8]. Among these, IrN_2 is the least compressible compound, with the highest bulk modulus (428 GPa) [6].

For Nb–N system, cubic δ-NbN superconducting phase possesses high bulk modulus (348 GPa) and Vickers hardness (20 GPa) closing to sapphire [9]. Jiang et al. [10] first proposed that U_2S_3 type Nb_2N_3 may be stable at wide pressures, and is a potential candidate for hard material. Recently, the phase diagram and mechanical properties of Nb–N system were analyzed by Zhao et al. [11]. They successfully predicted high pressure phases NbN_2 with orthorhombic structure (space group of *Cmca*, No. 64), which is thermodynamically stable up to 100 GPa, and meet mechanical and dynamical stability at ambient condition. The elastic constants, elastic modulus and density of states of NbN_2 have already been studied at ambient pressure. So far, however, the elastic constants, elastic anisotropy and especially thermodynamic properties of NbN_2 at high pressure have not been investigated, which is significant for their synthesis and practical applications [12]. Based on the above reasons, in this article, we focus on the detailed investigation on these fundamental properties of NbN_2 at various pressures and temperatures, including elastic constants, elastic anisotropy, and thermodynamic properties. We expect that our calculations can have guidable significances to accelerate the synthesis of NbN_2.

2. Computational method

In this paper, all first-principles calculations were performed with the CASTEP code [13]. Non-local ultrasoft pseudopotential (USPP) introduced by Vanderbilt [14] or norm-conserving pseudopotential (NCPP) presented by Hamann et al. [15] were employed for all ion–electron interactions. The Perdew–Burke–Ernzerhof (PBE) generalized gradient approximation (GGA) [16] and the local density approximation (LDA) proposed by Vosko et al. [17] were used to describe the exchange and correlation potentials. Pseudo-atomic calculations are performed for Nb: $4s^2 4p^6 4d^4 5s^1$ and N: $2s^2 2p^3$. The plane-wave basis set with energy cut-off of 550 eV, and $2\times6\times6$ Monkhorst-Pack grid for Brillouin zone sampling is used throughout. The structural optimizations were conducted using the Broyden–Fletcher–Goldfarb–Shanno (BFGS) minimization [18]. We found successfully the lowest energy structure, and the threshold of 5.0×10^{-6} eV/atom is used to determine whether the self-consistent progress has been converged.

Single crystal elastic constants were calculated via a strain–stress approach, i.e., by applying a small strain to the equilibrium lattice of orthorhombic unit cell and fitting the dependence of the resulting change in stress on the strain [12]. The elastic constants of c-W_3N_4 [19], TaN [20] and RuN_2 [21] were successfully obtained by using this method. This method is made as follows by a brief description.

In the elastic range, the orthorhombic crystal owns nine independent elastic coefficients C_{11}, C_{22}, C_{33}, C_{44},

*corresponding author; e-mail: lkworld@126.com

C_{55}, C_{66}, C_{12}, C_{13}, C_{23} because of the symmetry of the crystal. Elastic modulus values and the Poisson ratio can be obtained directly within these elastic constants based on the Voigt–Reuss–Hill method (VRH) [22], in which the Voigt and Reuss approximation is the theoretical maximum and minimum values. For the orthorhombic structure of NbN_2, the formulae as follows [23]:

$$\begin{aligned}
B_V &= [C_{11} + C_{22} + C_{33} + 2(C_{12} + C_{13} + C_{23})]/9,\\
G_V &= [C_{11} + C_{22} + C_{33} + 3(C_{44} + C_{55} + C_{66}\\
&\quad -(C_{12} + C_{13} + C_{23})]/15,\\
B_R &= \Delta/[C_{11}(C_{22} + C_{33} - 2C_{23}) + C_{22}(C_{33} - 2C_{13})\\
&\quad -2C_{33}C_{12} + C_{12}(2C_{23} - C_{12}) + C_{13}(2C_{12} - C_{13})\\
&\quad +C_{23}(C_{13} - C_{23}],\\
G_R &= \tfrac{15}{4}/\{[C_{11}(C_{22} + C_{33} + C_{23}) + C_{22}(C_{33} + C_{13})\\
&\quad +C_{33}C_{12} - C_{12}(C_{23} + C_{12}) - C_{13}(C_{12} + C_{13})\\
&\quad -C_{23}(C_{13} + C_{23})]/\Delta\\
&\quad +3(1/C_{44} + 1/C_{55} + 1/C_{66})\},
\end{aligned} \tag{1}$$

where

$$\begin{aligned}
\Delta &= C_{13}(C_{12}C_{23} - C_{13}C_{22} + C_{23}(C_{12}C_{13} - C_{23}C_{11})\\
&\quad +C_{33}(C_{11}C_{22} - C_{12}^2).
\end{aligned} \tag{2}$$

The Hill approximation represents the arithmetic mean values of the Voigt and Reuss approximation. The formulae are as follows [22]:

$$B_H = \tfrac{1}{2}(B_V + B_R), \tag{3}$$

$$G_H = \tfrac{1}{2}(G_V + G_R). \tag{4}$$

Once B and G are determined, the Young modulus E and the Poisson ratio v by the following formulae:

$$E = \frac{9B_H G_H}{3B_H + G_H}, \tag{5}$$

$$v = \frac{3B_H - 2G_H}{2(3B_H + G_H)}. \tag{6}$$

To investigate the thermodynamic properties, we here apply the quasi-harmonic Debye model [24]. In this model, the non-equilibrium Gibbs function $G^*(V; P, T)$ is as the following form:

$$G^*(V; P, T) = E(V) + PV + A_{vib}(\Theta_{\rm D}(V); T) \tag{7}$$

in which $E(V)$ is the total energy per unit cell for NbN_2; $\Theta_{\rm D}(V)$ is the Debye temperature; vibrational Helmholtz free energy A_{vib} can be written as [25–27]:

$$\begin{aligned}
A_{vib}(\Theta_{\rm D}; T) &= nk_{\rm B}T\\
&\quad \times \left(\frac{9}{8}\frac{\Theta_{\rm D}}{T} + 3\ln(1 - {\rm e}^{-\Theta_{\rm D}/T}) - D(\Theta_{\rm D}/T)\right),
\end{aligned} \tag{8}$$

where $D(\Theta_{\rm D}/T)$ represents the Debye integral, n is the number of atoms per formula unit and $k_{\rm B}$ is Boltzmann constant. Then the non-equilibrium Gibbs function $G^*(V; P, T)$, as a function of $(V; P, T)$, can be minimized with respect to volume V:

$$\left(\frac{\partial G^*(V; P, T)}{\partial V}\right)_{P,T} = 0. \tag{9}$$

We could obtain the thermal equation of state (EOS) by solving Eq. (9). Thus the isothermal bulk modulus B_T, the heat capacity C_V and the thermal expansion coefficient α are given by [28]:

$$B_T(P, T) = V\left(\frac{\partial^2 G^*(V; P, T)}{\partial V^2}\right)_{P,T}, \tag{10}$$

$$C_V = 3nk_{\rm B}\left(4D(\Theta_{\rm D}/T) - \frac{3\Theta_{\rm D}/T}{{\rm e}^{\Theta_{\rm D}/T} - 1}\right), \tag{11}$$

$$\alpha = \frac{\gamma C_V}{B_T V}, \tag{12}$$

$$\gamma = -\frac{{\rm d}\ln\Theta_{\rm D}(V)}{{\rm d}\ln V}, \tag{13}$$

where γ is the Grüneisen parameter.

3. Results and discussion

3.1. Equilibrium structure and elastic properties

Equilibrium lattice parameters, equilibrium volume and N–N bond length calculated by USPP GGA-PBE, GGA-PW91, LDA-CAPZ, NCPP GGA-PBE, together with the other calculated results of NbN_2, RuN_2, IrN_2 and Nb_2N_3 for comparison are listed in Table I. By USPP GGA-PBE the calculated lattice parameters a (12.333 Å), b (4.202 Å), c (4.120 Å) and equilibrium volume V (27.208 Å^3) for NbN_2 are in accordance with the theoretical data [11], and the differences between them are within about 1.31%, 0.51%, 0.52% and 2.32% for a, b, c axes and volume V, respectively. Good agreement between our computation results and other theoretical data provides a good support to investigate the elastic, anisotropy, and thermodynamic properties of NbN_2 under high pressures.

TABLE I

The calculated equilibrium lattice parameters a, b, c [Å], equilibrium volume V [Å^3], N–N length d [Å] for NbN_2 compounds (USPP GGA-PBE[a], GGA-PW91[b], LDA-CAPZ[c], NCPP GGA-PBE[d])

	a	b	c	V	d_{N-N}
NbN_2 [a]	12.333	4.202	4.120	27.208	1.366
[b]	12.291	4.213	4.209	27.243	1.374
[c]	12.075	4.152	4.151	26.010	1.367
[d]	12.565	4.270	4.263	28.585	1.348
[e]	12.496	4.224	4.222	27.854	1.325
RuN_2 [f]	4.098	4.919	2.696	54.344	1.379[g]
IrN_2 [h]	4.103	4.925	2.773	28.0	1.375
Nb_2N_3 [i]	8.20	8.31	3.02		1.32

[e] Ref. [11], PAW within GGA-PBE, [f] Ref. [21], USPP within GGA-PBE, [g] Ref. [29], USSP within GGA-PBE, [h] Ref. [23], GGA, [i] Ref. [10], PAW within GGA-PBE.

NbN_2 has not been synthesized in the laboratory, therefore, we list the elastic constants of several other transition metal nitrides hard materials RuN_2, IrN_2 and Nb_2N_3 for comparison in Table II.

TABLE II

Elastic coefficients C_{ij} [GPa] bulk modulus B [GPa] shear modulus G [GPa], the Young modulus E [GPa], B/G, the Poisson ratio v and Vickers hardness H_ν of NbN_2 from 0 to 100 GPa (USPP GGA-PBE[a], GGA-PW91[b], LDA-CAPZ[c]; NCPP GGA-PBE[d] at 0 GPa).

	P	C_{11}	C_{22}	C_{33}	C_{44}	C_{55}	C_{66}	C_{12}	C_{13}	C_{23}	B	G	E	B/G	ν	H_ν
NbN_2 [a]	0	635	609	621	308	57	74	117	94	241	307	149	385	2.057	0.291	22.36
[b]	0	512	602	617	317	51	37	159	137	218	301	123			0.32	
[c]	0	742	710	715	310	119	113	131	119	268	355	198			0.27	
[d]	0	658	590	590	262	44	29	101	92	201	292	118			0.32	
[e]	0	577	597	596	294	54	54	108	112	231	295	134			0.30	
	10	705	684	701	327	83	96	153	124	270	353	176	454	2.000	0.286	22.75
	20	781	756	777	348	107	113	186	153	297	398	201	516	1.980	0.284	22.34
	30	856	826	850	367	126	131	215	181	323	441	223	572	1.979	0.284	22.44
	40	932	896	919	384	144	146	241	208	347	482	243	623	1.986	0.284	22.34
	50	1002	996	995	392	159	160	250	245	352	520	263	675	1.979	0.284	21.40
	60	1064	1062	1058	404	172	173	275	272	375	558	279	717	2.001	0.286	21.08
	70	1126	1126	1122	415	184	185	300	298	400	596	294	758	2.027	0.288	20.55
	80	1188	1189	1184	427	196	197	324	324	423	633	309	797	2.050	0.290	18.95
	90	1251	1250	1244	437	208	209	348	349	446	670	323	835	2.071	0.292	19.38
	100	1313	1310	1306	447	219	220	372	373	469	706	337	873	2.092	0.294	17.31
RuN_2 [f]	0	642	783	524	113	283	152	160	216	45	306	196	484	1.562	0.236	13.66[g]
IrN_2 [h]	0	739	883	554	124	297	190	156	277	82	345	217	538		0.240	17.92[g]
Nb_2N_3 [i]	0	426	549	582	152	169	96	237	188	168	303	143	370		0.297	

[e]Ref. [11], PAW within GGA-PBE, [f]Ref. [21], USPP within GGA-PBE, [g]Ref. [29], USSP within GGA-PBE, [h]Ref. [23], GGA, [i]Ref. [10], PAW within GGA-PBE.

The LDA method to some extent overestimates the elastic constants [30]. It can be seen from the table that the LDA-calculated elastic coefficients are significantly larger than the other theoretical value. Correspondingly, the shear modulus G is also distinct greater than the other theoretical value. On the other hand, the results of GGA-PBE and GGA-PW91 are in good agreement with the values in Ref. [11]. As is known to all, the requirement of mechanical stability in an orthorhombic crystal leads to the following restrictions on the elastic constants [21]:

$$C_{11} > 0,\ C_{22} > 0,\ C_{33} > 0,\ C_{44} > 0,$$

$$C_{55} > 0,\ C_{66} > 0,\ C_{11} + C_{22} - 2C_{12} > 0,$$

$$C_{11} + C_{33} - 2C_{13} > 0,\ C_{22} + C_{33} - 2C_{23} > 0.$$

$$[C_{11} + C_{22} + C_{33} + 2(C_{12} + C_{12} + C_{23})] > 0. \qquad (14)$$

The elastic constants C_{ij} of NbN_2 as a function of pressure are plotted in Fig. 1. In the range of less than 100 GPa, all elastic coefficients C_{ij} are in line with the stability criteria, which indicates that NbN_2 is mechanically stable under high pressure. Then all elastic coefficients increase linearly with the increase of pressure. Moreover, C_{11}, C_{22}, C_{33} reflect the bond strength in the $\langle 001\rangle$, $\langle 010\rangle$, $\langle 100\rangle$ direction. In Fig. 1, the elastic constants C_{11}, C_{22}, C_{33} are distinctly larger than others and tend to be almost equal at high pressure.

Furthermore, it is also found that elastic constants of NbN_2 are almost comparable with them of RuN_2, IrN_2 and Nb_2N_3 i.e., elastic properties of NbN_2 is comparable to other potential (super)hard materials, which indicate that NbN_2 is a potential incompressible and hard material. In general, the shear modulus is a better indicator of hardness in the design of novel hard/superhard materials because it ultimately measures the plastic deformation under indentations [31, 32]. Table II lists all the elastic moduli of NbN_2 under different pressures. Obviously, the values of the bulk modulus B, shear modulus G and the Young modulus E increase substantially with

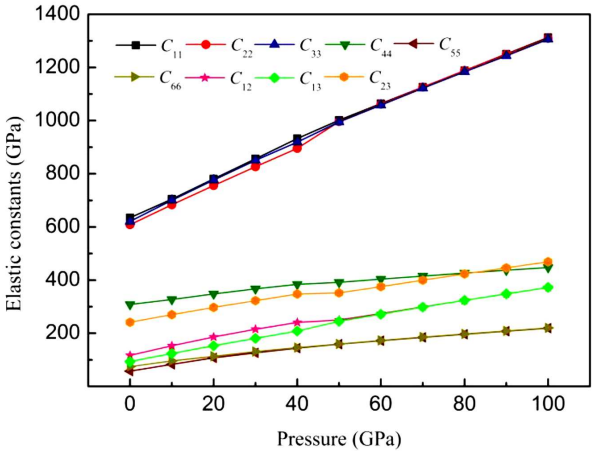

Fig. 1. Pressure dependence of the elastic coefficients (C_{ij}) of NbN_2.

pressure. The calculated elastic moduli, especially shear moduli (149 GPa) of NbN_2 are comparable to those of RuN_2 (196 GPa), IrN_2 (217 GPa) and Nb_2N_3 (143 GPa). Further to check our conjecture, the hardness calculation seems to be of interest and necessary. The intrinsic hardness of NbN_2 compounds were calculated by the formula of Gao [33]. The intrinsic hardness of ReN_2, WN_2 [34], PtN_2 [35] and IrN_2, RuN_2 [29] were successfully obtained by applying this method. The calculated hardness values of orthorhombic NbN_2 are 22.36 GPa, which is larger that of RuN_2 (13.66 GPa) and IrN_2 (17.92 GPa). The fact further suggests NbN_2 is a candidate for hard material.

B/G and the Poisson ratio ν, listed in Table II are used to judge ductility of materials. According to the Pugh criterion [36] if $B/G > 1.75$, the material behaves in a ductile manner otherwise, the material behaves in a brittle manner. It can be clearly seen in Table II that the NbN_2 is strongly prone to ductile under high pressure, which is consistent with the result judged by the Poisson ratio ν that can be judgment of ductility and brittleness, for a brittle material $\nu < 0.26$, while for a ductile material $\nu > 0.26$ [37].

As a fundamental parameter of a solid, the Debye temperature Θ_{D} correlates with many physical properties of solid materials, such as vibrational internal energy and elastic constants. The Θ_{D} can be calculated from elastic constants by the following formula [38]:

$$\Theta_{\mathrm{D}} = \frac{h}{k_{\mathrm{B}}} \left(\frac{3n}{4\pi} \frac{N_{\mathrm{A}}\rho}{M} \right)^{\frac{1}{3}} \nu_m, \tag{15}$$

which gives explicit information about the lattice vibrations [39]. The calculated shear wave velocity, longitudinal wave velocity, average sound velocity and the Debye temperature of NbN_2 compounds at zero, high pressure and zero temperature are presented in Table III, presenting a trend of increase with pressure. The calculated Debye temperature of NbN_2 at 0 K and 0 GPa is 715 GPa, which is larger than that of Nb_2N_3 (666 K) [10].

TABLE III

The calculated density ρ [g cm^{-3}], the longitudinal, transverse and mean elastic wave velocity (ν_l, ν_t and ν_m [m/s], and the Debye temperature Θ_{D} [K] of NbN_2 under pressure.

P	ρ	ν_l	ν_t	ν_m	Θ_{D}
0	7.38	8277	4495	5015	715.77
10	7.60	8793	4817	5370	774.18
20	7.81	9231	5071	5653	822.13
30	8.00	9603	5277	5882	862.21
40	8.17	9927	5449	6074	896.85
50	8.33	10221	5617	6261	930.57
60	8.49	10467	5732	6391	955.85
70	8.64	10698	5836	6509	979.06
80	8.78	10911	5932	6618	1000.88
90	8.92	11111	6022	6719	1021.39
100	9.05	11304	6108	6817	1041.23

3.2. Elastic anisotropy

Elastic anisotropy analysis is of great significance in understanding the mechanisms of materials microcracks, phase transformations, elastic instability and durability [40]. Hence, a proper description of such an anisotropic behavior is important in engineering science as well as in crystal physics. The universal elastic anisotropy index A^U, the shear anisotropy factors (A_G, A_1, A_2, A_3) and the bulk modulus anisotropy factors A_B, B_a, B_b and B_c are appropriate measures to quantify the extent of anisotropy [41].

Firstly, the universal elastic anisotropy index A^U, which can provide theoretical basis for the degree of anisotropy, is defined by Ranganathan and Ostoja-Starzewski from the bulk modulus B and shear modulus G by Voight and Reuss approaches [41], as

$$A^U = 5\frac{G_V}{G_R} + \frac{B_V}{B_R} - 6. \tag{16}$$

Secondly, the percent shear and compressibility modulus factors in polycrystalline materials which can be defined as [42]:

$$A_G = \frac{G_V - G_R}{G_V + G_R},\ A_B = \frac{B_V - B_R}{B_V + B_R}. \tag{17}$$

In addition, for orthorhombic crystals, the shear anisotropic factor for the $\langle 100 \rangle$ shear planes between the $\langle 011 \rangle$ and $\langle 010 \rangle$ directions is [41]:

$$A_1 = \frac{4C_{44}}{C_{11} + C_{33} - 2C_{13}}, \tag{18}$$

for the $\langle 010 \rangle$ shear planes between $\langle 101 \rangle$ and $\langle 001 \rangle$ directions is

$$A_2 = \frac{4C_{55}}{C_{22} + C_{33} - 2C_{23}}, \tag{19}$$

for the $\langle 001 \rangle$ shear planes between $\langle 110 \rangle$ and $\langle 010 \rangle$ directions is

$$A_3 = \frac{4C_{66}}{C_{11} + C_{22} - 2C_{12}}. \tag{20}$$

Meanwhile, the directional bulk modulus along different crystallographic axis can be defined as [42]:

$$B_i = i(\mathrm{d}P/\mathrm{d}i)\ (i = a, b, \text{ and } c). \tag{21}$$

The anisotropy of the bulk modulus along the a-axis and c-axis with respect to b-axis can be defined by:

$$A_{B_a} = B_a/B_b,\ A_{B_c} = B_c/B_b. \tag{22}$$

Based on the formulae mentioned above, the calculated values of A^U, A_G, and A_B are plotted in Fig. 2. For these three expressions, a value of zero represents elastic isotropy and a value of 1 (100%) is largest possible anisotropy. At 0 GPa, $A^U = 2.852$, it indicates that NbN_2 is anisotropic materials. In general, A^U, A_G and A_B decreases with increase of pressure and that is to say extent of anisotropy of NbN_2 will be decreased with increase of pressure. A_B is almost equal to 0 at high pressure which suggests NbN_2 is slightly isotropic in compressibility. Namely, bulk modulus anisotropy is evidently smaller than that of shear modulus anisotropy.

The values of A_1, A_2, A_3 and A_{Ba}, A_{Bc} equal to 1.0 mean that the crystal is isotropic and the degree of the

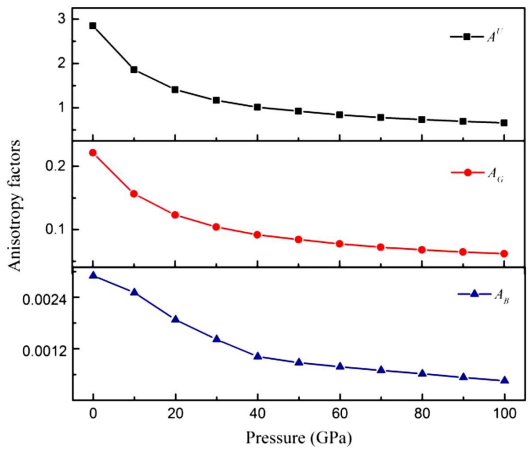

Fig. 2. Anisotropy factors (A^U, A_G, A_B) of NbN_2 as functions of pressure.

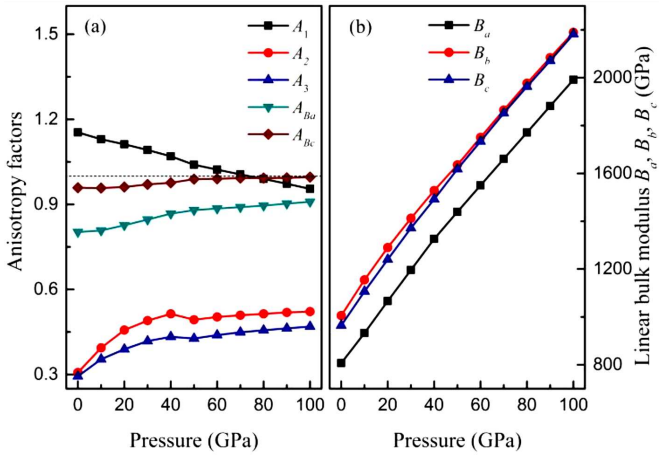

Fig. 3. Anisotropy factors (A_1, A_2, A_3 and A_{Ba}, A_{Bc}) and linear bulk modulus (B_a, B_b, B_c) of NbN_2 as functions of pressure (in which the dotted line represents one).

elastic anisotropy can be reflected by the deviation from one. Then these parameters are plotted as a function of pressure in Fig. 3a. When pressure is increased from 0 to 100 GPa, the shear anisotropy factors A_1 decrease by 17.2% and A_2, A_3 increase by 70.3% and 59.5%, respectively. This change is mainly caused by the change of the elastic constants, especially for A_1 the C_{44} only increases by 17.2%, but for A_2 the C_{55} and A_3 the C_{66} increase by 284% and 197%, respectively. The anisotropy of the linear bulk modulus A_{Bb} and A_{Bc} increases by 13.3% and 3.9%, respectively. Meanwhile, in Fig. 3b, it is interesting to note that the directional bulk modulus B_b along the b axis is largest when compared to the B_a and B_c at 0 GPa, and B_c is close to B_b along with pressure increase.

To characterize the degree of anisotropy of the Young modulus, drawing a three-dimensional (3D) graph for NbN_2 compounds is necessary. The three-dimensional formulas for the Young modulus E in the orthorhombic system [42] are expressed as follows:

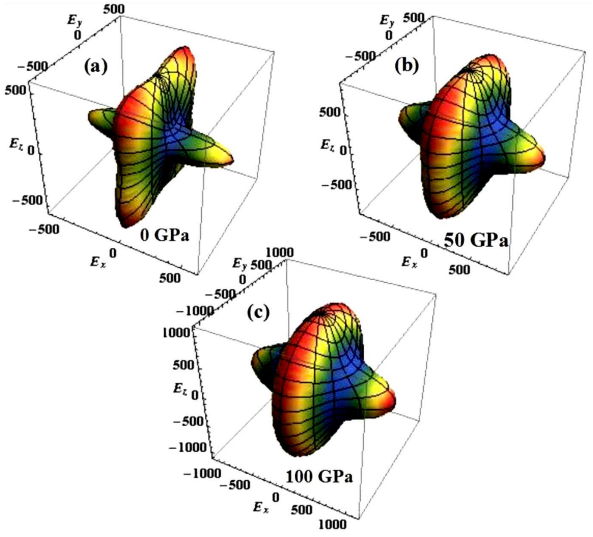

Fig. 4. Direction dependence of the Young modulus E under different pressures for NbN_2, the units are in GPa for E.

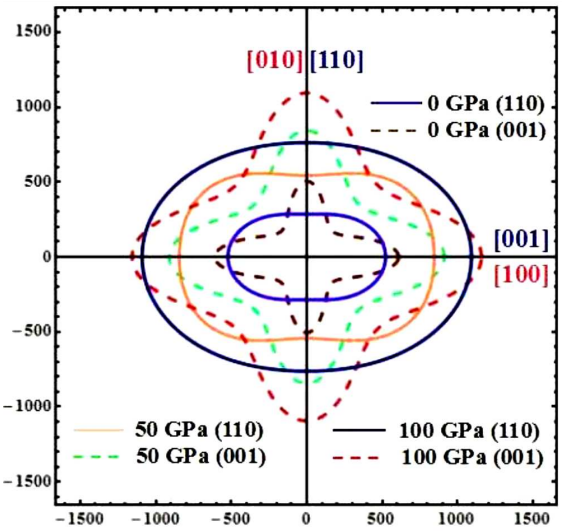

Fig. 5. The projections of the Young modulus E [GPa] in (110) plane and (001) plane at pressures 0, 50, and 100 GPa, respectively.

$$E^{-1} = s_{11}l_1^4 + s_{22}l_2^4 + s_{33}l_3^4 + 2s_{12}l_1^2l_2^2 + 2s_{23}l_2^2l_3^2$$
$$+2s_{13}l_1^2l_3^2 + s_{44}l_2^2l_3^2 + s_{55}l_1^2l_3^2 + s_{66}l_1^2l_2^2, \quad (23)$$

where s_{ij} is the usual elastic compliance constants and l_i is the direction cosines in any arbitrary direction. The 3D graph of the Young modulus at three pressures is shown in Fig. 4. From Fig. 4, the Young modulus anisotropy of NbN_2 is described in detail and the degree of anisotropy will decrease when pressure increases. At 50, 100 GPa, the values of the Young modulus in $\langle 100 \rangle$, $\langle 010 \rangle$, and $\langle 001 \rangle$ direction is almost equal and greater than that of other direction. Because a larger Young modulus often stands for more covalent feature of a material [43, 44], the facts indicate that the strength of chemical bonds in

⟨100⟩, ⟨010⟩ and ⟨001⟩ direction is stronger than other directions at high pressure, which is consistent with the results of analysis of elastic constants. Furthermore, the direction dependence of E in (001) plane and in (110) plane at 0, 50, and 100 GPa also are shown in Fig. 5.

3.3. Thermodynamic properties

We calculated energy–volume points at 0 K and 0 GPa by compressive and tensile lattice constants under the same proportion. Then, thermodynamic quantities of NbN_2 at different temperatures (0, 500, 1000, 1500, 2000, and 2500 K) and pressures were obtained through the quasi-harmonic Debye model.

As one of the most important thermodynamic parameters, the special heat capacity C_V of a substance not only provides essential information about its vibrational properties but also is fundamental to many applications [45]. The heat capacity C_V of NbN_2 at different temperatures and pressure are presented in Fig. 6. It shows the heat capacity C_V increases with the increase of temperature, while decreases as pressure increases. At low temperature ($\approx$ 500 K), the heat capacity C_V is dependent on both temperature and pressure, which is owing to the anharmonic approximations of the Debye model [24]. At high temperatures, C_V of all solid will nearly approach to the Dulong–Petit limit $3nN_Ak_B$ (n represents the numbers of atoms in the molecule). As temperature increases, the heat capacity C_V is close to the Dulong–Petit limit $3nN_Ak_B$ ($\approx$ 299.32 J mol^{-1} K^{-1}), where $n = 12$ for NbN_2 in unit cell.

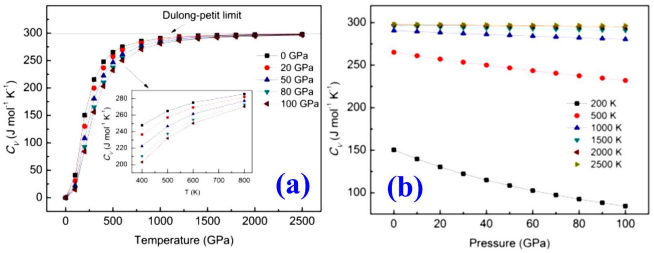

Fig. 6. The heat capacity C_V of NbN_2 as functions of temperature and pressure.

TABLE IV

Values of the Debye temperature Θ_D, entropy S and Grüneisen parameter γ of NbN_2 at different temperatures.

T [K]		P [GPa]										
		0	10	20	30	40	50	60	70	80	90	100
0	Θ_D	802	851	896	937	975	1011	1045	1077	1108	1137	1165
	S	0.0	0.0	0.0	0.0	0.0	0.0	0.0	0.0	0.0	0.0	0.0
	γ	2.041	1.985	1.936	1.893	1.854	1.819	1.786	1.756	1.728	1.702	1.677
200	Θ_D	801	850	895	936	974	1011	1045	1077	1108	1137	1165
	S	77.9	69.3	62.3	56.6	51.9	47.8	44.3	41.3	38.6	36.2	34.1
	γ	2.043	1.986	1.937	1.894	1.855	1.82	1.787	1.757	1.729	1.703	1.678
500	Θ_D	790	840	886	928	967	1004	1039	1071	1103	1132	1161
	S	280.2	264.0	250.1	238.2	227.8	218.6	210.2	202.8	195.9	189.7	183.9
	γ	2.056	1.997	1.946	1.902	1.862	1.826	1.793	1.762	1.733	1.707	1.682
1500	Θ_D	740	795	845	891	933	972	1009	1043	1076	1107	1136
	S	612.3	591.0	573.1	557.5	544.0	532.0	521.2	511.3	502.4	494.1	486.4
	γ	2.12	2.049	1.991	1.941	1.897	1.858	1.822	1.788	1.758	1.729	1.703
2500	Θ_D	681	745	800	849	895	937	975	1012	1046	1079	1110
	S	788.7	762.2	741.0	723.1	707.5	694.0	682.0	671.1	661.1	652.1	643.6
	γ	2.211	2.114	2.044	1.987	1.937	1.894	1.855	1.819	1.786	1.755	1.727

Thermal expansion coefficient α as functions of pressure (temperature) are shown in Fig. 7. In Fig. 7a, it is noted that the α increases quickly with temperature at low pressure and temperatures and the trend of increase will become slow at high temperatures. Specifically, temperature increases from 0 to 600 K at 20 GPa, α increases from 0 to 2.14×10^{-5} K^{-1}. But α only increases 0.78×10^{-5} K^{-1} when temperature rises from 600 K to 2500 K. It is clearly seen that the curves at high temperature is very close in Fig. 7b. Additionally, the Debye temperature Θ_D, entropy S and Grüneisen parameter γ of NbN_2 along with the change of pressure and temperature were also calculated, which were listed in Table IV. It is obvious that Θ_D rises with the increase of pressure and reduces with increase of temperature conversely. Meanwhile, pressure has a more evident influence on Θ_D than temperature.

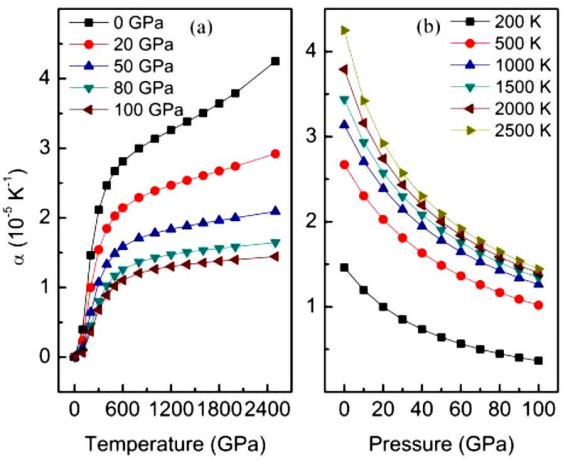

Fig. 7. The thermal expansion α versus temperature and pressure.

4. Conclusions

The elastic, anisotropy, and thermodynamic properties of the NbN_2 at high pressure were investigated and evaluated by the first-principles calculations. The obtained data of the ground state structural properties are in excellent agreement with reliable theoretical results. The calculated elastic properties and intrinsic hardness for NbN_2 show that it is almost competitive with hard materials RuN_2, IrN_2, and Nb_2N_3, which indicate that NbN_2 is a potential hard material. According to the Born stability criteria and the Pugh criterion, NbN_2 is mechanically stable and a ductile material at 0–100 GPa, respectively. NbN_2 possesses distinct elastic anisotropy and the degree of anisotropy will reduce with increasing pressure. Through the quasi-harmonic Debye model, special heat capacity C_V and thermal expansion α as functions of pressure and temperature, dependences of Debye temperature Θ_D entropy S and Grüneisen parameter γ on pressure and temperature have also been analyzed.

Acknowledgments

This work is supported by the international cooperation projects Foundation of SiChuan Provincial Science and Technology Department (Grant No. 2014HH0014) and the Scientific Research Fund of SiChuan Provincial Education Department (Grant No. 15ZA0033), and the Project funded by China Postdoctoral Science Foundation (Grant No. 2016M602666).

References

[1] A.Y. Liu, M.L. Cohen, *Science* **245**, 841 (1989).

[2] J.L. He, L.C. Guo, D.L. Yu, R.P. Liu, Y.J. Tian, H. Tian, *Appl. Phys. Lett.* **85**, 5571 (2004).

[3] Y. Liang, C. Li, W. Guo, W. Zhang, *Phys. Rev. B* **79**, 024111 (2009).

[4] E. Gregoryanz, C. Sanloup, M. Somayazulu, J. Badro, G. Fiquet, H.K. Mao, R.J. Hemley, *Nat. Mater.* **3**, 294 (2004).

[5] J.C. Crowhurst, A.F. Goncharov, B. Sadigh, C.L. Evans, P.G. Morrall, J.L. Ferreira, A.J. Nelson, *Science* **311**, 1275 (2006).

[6] A.F. Young, C. Sanloup, E. Gregoryanz, S. Scandolo, R.J. Hemley, H.K. Mao, *Phys. Rev. Lett.* **96**, 155501 (2006).

[7] J.C. Crowhurst, A.F. Goncharov, B. Sadigh, J.M. Zaug, D. Aberg, Y. Meng, V.B. Prakapenka, *J. Mater. Res.* **23**, 1 (2008).

[8] A. Friedrich, B. Winkler, E.A. Juarez-Arellano, L. Bayarjargal, *Materials* **4**, 1648 (2011).

[9] X.J. Chen, V.V. Struzhkin, Z. Wu, M. Somayazulu, J. Qian, S. Kung, A.N. Christensen, Y. Zhao, R.E. Cohen, H.K. Mao, R.J. Hemley, *Proc. Natl. Acad. Sci. U.S.A.* **102**, 3198 (2005).

[10] C. Jiang, Z. Lin, Y. Zhao, *Scr. Mater.* **63**, 532 (2010).

[11] Z.L. Zhao, K. Bao, F.B. Tian, X.L. Jin, D.F. Duan, D. Li, X.L. Huang, B.B. Liu, T. Cui, *Phys. Chem. Chem. Phys.* **17**, 22837 (2015).

[12] R. Hao, X. Zhang, J. Qin, S. Zhang, J. Ning, N. Sun, M. Ma, R. Liu, *RSC Adv.* **5**, 36779 (2015).

[13] M.D. Segall, P.J.D. Lindan, M.J. Probert, C.J. Pickard, P.J. Hasnip, S.J. Clark, M.C. Payne, *J. Phys. Condens. Matter* **14**, 2717 (2002).

[14] D. Vanderbilt, *Phys. Rev. B* **41**, 7892 (1990).

[15] D.R. Hamann, M. SchlÜter, C. Chiang, *Phys. Rev. Lett.* **43**, 1494 (1979).

[16] J.P. Perdew, K. Burke, M. Ernzerhof, *Phys. Rev. Lett.* **77**, 3865 (1996).

[17] S.H. Vosko, L. Wilk, M. Nussair, *Can. J. Phys.* **58**, 1200 (1980).

[18] B.G. Pfrommer, M. Côté, S.G. Louie, M.L. Cohen, *J. Comp. Physiol.* **131**, 233 (1997).

[19] K. Liu, S.M. Wang, X.L. Zhou, J. Chang, *J. Appl. Phys.* **114**, 063512 (2013).

[20] J. Chang, G.P. Zhao, X.L. Zhou, K. Liu, L.Y. Lu, *J. Appl. Phys.* **112**, 083519 (2012).

[21] B. Dong, X.L. Zhou, K. Liu, J. Chang, *J. Appl. Phys.* **116**, 053511 (2014).

[22] R. Hill, *Proc. Phys. Soc. Lond.* **65**, 350 (1952).

[23] Z.J. Wu, E.J. Zhao, H.P. Xiang, X.F. Hao, J. Liu, J. Meng, *Phys. Rev. B* **76**, 054115 (2007).

[24] M.A. Blanco, E. Francisco, V. Luaña, *Comput. Phys. Commun.* **158**, 57 (2004).

[25] A.A. Maradudin, E.W. Montroll, G.H. Weiss, I.P. Ipatova, *Theory of Lattice Dynamics in the Harmonic Approximation*, Academic Press, New York 1971.

[26] M.A. Blanco, A.M. Pendás, E. Francisco, J.M. Recio, R. Franco, *J. Mol. Struct.* **368**, 245 (1996).

[27] M. Flórez, J.M. Recio, E. Francisco, M.A. Blanco, A.M. Pendás, *Phys. Rev. B* **66**, 144112 (2002).

[28] E. Francisco, M.A. Blanco, G. Sanjurjo, *Phys. Rev. B* **63**, 094107 (2001).

[29] B. Dong, K. Liu, X.L. Zhou, J. Tan, X.C. Mao, J. Chang, *Phys. Status Solidi B* **253**, 527 (2016).

[30] C. Stampfl, W. Mannstadt, R. Asahi, A.J. Freeman, *Phys. Rev. B* **63**, 155106 (2001).

[31] V.V. Brazhkin, A.G. Lyapin, R.J. Hemley, *Philos. Mag. A* **82**, 231 (2002).

[32] R.B. Kaner, J.J. Gilman, S.H. Tolbert, *Science* **308**, 1268 (2005).

[33] F.M. Gao, *Phys. Rev. B* **73**, 132104 (2006).

[34] X.P. Du, Y.X. Wang, V.C. Lob, *Phys. Lett. A* **374**, 2569 (2010).

[35] H.Y. Gou, L. Hou, J.W. Zhang, G.F. Sun, L.H. Gao, F.M. Gao, *Appl. Phys. Lett.* **89**, 141910 (2006).

[36] S.F. Pugh, *Philos. Mag.* **45**, 823 (1954).

[37] J.J. Lewandowski, W.H. Wang, A.L. Greer, *Philos. Mag. Lett.* **85**, 77 (2005).

[38] O.L. Anderson, *J. Phys. Chem Solids* **24**, 909 (1963).

[39] J. Jia, D. Zhou, J. Zhang, F. Zhang, Z. Lu, C. Pu, *Comput. Mater. Sci.* **95**, 228 (2014).

[40] Y.H. Duan, Y. Sun, M.J. Peng, S.G. Zhou, *J. Alloys Comp.* **595**, 14 (2014).

[41] S.I. Ranganathan, M. Ostoja-Starzewski, *Phys. Rev. Lett.* **101**, 055504 (2008).

[42] P. Ravindran, L. Fast, P. Korzhavyi, B. Johansson, J. Wills, O. Eriksson, *J. Appl. Phys.* **84**, 4891 (1998).

[43] M. Rajagopalan, S.P. Kumar, R. Anuthama, *Physica B* **405**, 1817 (2010).

[44] G. Yi, X. Zhang, J. Qin, J. Ning, S. Zhang, M. Ma, R. Liu, *J. Alloys Comp.* **640**, 455 (2015).

[45] X.Y. Zhang, J.Q. Qin, J.L. Ning, X.W. Sun, X.T. Li, M.Z. Ma, R.P. Liu, *J. Appl. Phys.* **114**, 183517 (2013).